The Astrophysical Journal Letters, 810:L14 (6pp), 2015 September 10 doi:10.1088/2041-8205/810/2/L14

HIGH-*J* CO VERSUS FAR-INFRARED RELATIONS IN NORMAL AND STARBURST GALAXIES

Daizhong Liu[1,2,3], Yu Gao[1], Kate Isaak[4], Emanuele Daddi[3], Chentao Yang[1,2,5], Nanyao Lu[6], and Paul van der Werf[7]
[1] Purple Mountain Observatory/Key Laboratory for Radio Astronomy, Chinese Academy of Sciences, Nanjing, China; yugao@pmo.ac.cn
[2] University of Chinese Academy of Sciences, Beijing, China
[3] CEA Saclay, Laboratoire AIM-CNRS-Université Paris Diderot, IRFU/SAp, Orme des Merisiers, F-91191 Gif-sur-Yvette, France
[4] Scientific Support Office, ESTEC/SRE-S Keplerlaan 1, NL-2201 AZ, Noordwijk, The Netherlands
[5] Institut d'Astrophysique Spatiale, Bât 121, Université Paris-Sud, F-91405 Orsay, France
[6] Infrared Processing and Analysis Center, California Institute of Technology, MS 100-22, Pasadena, CA 91125, USA
[7] Leiden Observatory, Leiden University, Post Office Box 9513, NL-2300 RA Leiden, The Netherlands
Received 2015 May 20; accepted 2015 August 2; published 2015 September 1

ABSTRACT

We present correlations between 9 CO transitions ($J = 4$–3 to 12–11) and beam-matched far-infrared (far-IR) luminosities ($L_{\rm FIR,\it b}$) among 167 local galaxies, using *Herschel* Spectral and Photometric Imaging Receiver Fourier Transform Spectrometer (SPIRE; FTS) spectroscopic data and Photoconductor Array Camera and Spectrometer (PACS) photometry data. We adopt entire-galaxy FIR luminosities ($L_{\rm FIR,\it e}$) from the *IRAS* Revised Bright Galaxy Sample and correct to $L_{\rm FIR,\it b}$ using PACS images to match the varying FTS beam sizes. All 9 correlations between $L'_{\rm CO}$ and $L_{\rm FIR,\it b}$ are essentially linear and tight ($\sigma = 0.2$–0.3 dex dispersion), even for the highest transition, $J = 12$–11. This supports the notion that the star formation rate (SFR) is linearly correlated with the dense molecular gas ($n_{\rm H_2} \gtrsim 10^{4-6}$ cm^{-3}). We divide the entire sample into three subsamples and find that smaller sample sizes can induce large differences in the correlation slopes. We also derive an average CO spectral line energy distribution for the entire sample and discuss the implied average molecular gas properties for these local galaxies. We further extend our sample to high-z galaxies with CO($J = 5$–4) data from the literature as an example, including submillimeter galaxies (SMGs) and "normal" star-forming BzKs. BzKs have similar FIR/CO(5–4) ratios as those of local galaxies, and agreeably follow the locally-determined correlation, whereas SMG ratios fall around or slightly above the local correlation with large uncertainties. Finally, by including Galactic CO($J = 10$–9) data as well as very limited high-z CO($J = 10$–9) data, we verify that the CO($J = 10$–9)–FIR correlation successfully extends to Galactic young stellar objects, suggesting that linear correlations are valid over 15 orders of magnitude.

Key words: galaxies: ISM – galaxies: starburst – infrared: ISM – ISM: molecules

1. INTRODUCTION

Molecular gas is the raw material from which stars are formed, hence its presence and physical conditions correlate with the star formation rate (SFR). A well-known correlation between gas surface density and SFR surface density is the *Kennicutt–Schmidt law* (K–S law): $\Sigma_{\rm SFR} = A\,\Sigma_{\rm gas}^{N}$, with a slope $N = 1.4 \pm 0.15$ (Kennicutt 1998), where $\Sigma_{\rm SFR}$ is based on H_α luminosity or far-infrared (far-IR) luminosity ($L_{\rm FIR}$, 40–400 μm) and $\Sigma_{\rm gas}$ is the sum of the atomic gas (from HI observations) and molecular gas (inferred from CO(1–0) line luminosity) surface density. This quantitative correlation serves as a fundamental input to most cosmological simulations (e.g., Springel & Hernquist 2003; Mac Low & Klessen 2004; Krumholz & McKee 2005; Krumholz & Thompson 2007; Narayanan et al. 2008). However, it brushes over and/or oversimplifies the relationship between the individual gas components and star formation (SF). First, observations have shown that the presence and state of the atomic gas component has little impact on SF (e.g., Bigiel et al. 2008; Liu & Gao 2012; Schruba 2013; Liu et al. 2015). Second, the correlation between the most widely used molecular gas tracer, CO(1–0), and $L_{\rm FIR}$ is found to be more complex than just a single power law: Gao & Solomon (2004) showed that the CO (1–0)–FIR slope changes from 1.27 to 1.73 with different sample selections, e.g., including only normal star-forming galaxies (SFGs: $L_{\rm IR} < 10^{11}\,L_\odot$), or adding (ultra-)luminous IR galaxies (LIRGs: $L_{\rm IR} = 10^{11-12}\,L_\odot$; ULIRGs: $L_{\rm IR} > 10^{13}\,L_\odot$), respectively. Greve et al. (2014, hereafter G14) showed similar slope variations from 0.9 to 1.4 by analyzing a large number of data from the literature. It is thus questionable that a single power-law relation exists between CO(1–0) and FIR and whether it can be applied to all galaxies even if it exists.

CO(1–0) has a low critical density ($n_{\rm H_2,crit} \sim 2 \times 10^3$ cm^{-3}), and thus traces the total amount of molecular gas. It provides no physical insight into the higher density gas ($n_{\rm H_2} > 10^4$ cm^{-3}) that is known to be found at the formation sites of individual stars (Kennicutt & Evans 2012). The sensitivity of the CO ($J_u \rightarrow J_u - 1$) transition to denser/warmer gas increases with an increasing upper level (J_u): for example, CO(10–9) has a critical density of $n_{\rm H_2,crit} \sim 10^6$ cm^{-3} (Carilli & Walter 2013). In contrast, the ground-J of high dipole-moment molecules such as HCN and HCO^+ already have $n_{\rm H_2,crit} \sim 10^6$ cm^{-3}, thus probing the dense gas in cold phase. Studies based on HCN (Gao & Solomon 2004; Wu et al. 2005, 2010) and high-J CS (Zhang et al. 2014) have found a unified linear correlation between dense gas and the SFR, describing the scenario in which all dense gas above a certain density threshold has a similar efficiency/timescale to collapse and form new stars, thus linearly determining SFRs.

Until recently, published mid-to-high-J ($J_u \geqslant 4$) CO data in local galaxies were still scarce due to the challenges of observing at frequencies $\gtrsim$450 GHz from the ground. Bayet et al. (2009) performed large velocity gradient (LVG) modeling with ground-based $J_u \leqslant 7$ CO to extrapolate $J_u > 7$ transitions for several local galaxies. They found that CO versus total IR luminosity ($L_{\rm TIR}$, 8–1000 μm) correlations have decreasing slopes for increasing J_u, similar to what modelings and simulations predicted (Narayanan et al. 2008; Juneau et al. 2009).

More recently, G14 presented the *Herschel* Spectral and Photometric Imaging Receiver (SPIRE; Griffin et al. 2010) Fourier Transform Spectrometer (FTS, Naylor et al. 2010) high-J CO data from the HerCULES program (Van der Werf et al. 2010; Rosenberg et al. 2015). They find that up to CO (7–6) the CO versus TIR or FIR relations are all roughly linear, while for higher-J_u the correlations become sub-linear, similar to the results of Bayet et al. (2009).

In this work, we use a large SPIRE FTS data set to statistically determine the correlations between 9 $L'_{\rm CO}$ (J = 4–3 to 12–11) and beam-matched $L_{{\rm FIR},b}$, and to determine which transitions are the best tracers of SF. We also verify the slope variations against J_u and test the validity of dense gas versus SF relation at high-z. The sample, data, and method are described in Section 2. The results and a discussion are given in Section 3. We adopt $H_0 = 73\ {\rm km\ s^{-1}}$, $\Omega_\Lambda = 0.73$, $\Omega_M = 0.27$.

2. SAMPLE AND DATA

The sample was selected from all public FTS observations in the *Herschel* Science Archive (HSA) of local galaxies that are in the *IRAS* Revised Bright Galaxy Sample (Sanders et al. 2003). A further selection criterion requiring the availability of 70–160 μm band imaging data taken with Photoconductor Array Camera and Spectrometer (PACS, Poglitsch et al. 2010) for galaxies partially resolved by the FTS beam (see Section 2.1) was imposed to enable beam-matching techniques to be used in the analysis. The final sample contains 167 local galaxies ($z < 0.064$, $d_L < 286$ Mpc), including 124 (U)LIRGs and 43 SFGs (see Rosenberg et al. (2015) and Lu et al. (2014) for details of the HerCULES and GOALS programs, respectively; details of the full data set are given in D. Liu et al. (2015, in preparation).

2.1. FTS CO Measurements

FTS has two bolometer arrays: the SLW bolometer array (446–989 GHz) and the SSW bolometer array: (959–1543 GHz). Two observing modes are used: single-pointing for point-like sources (mostly with angular size less than FTS beam sizes, and $d_L > 30$ Mpc), and mapping for nearby extended sources ($d_L < 30$ Mpc). In single-pointing observations the central bolometer of each array is coaligned with the target, while off-axis bolometers point to the off-center sky. Mapping observations perform jiggling to scan extended targets, and each individual bolometer will produce one spectrum at its own pointing (R.A., decl.). All mapping data and ∼30% single-pointing data were reduced using SPIRE v12 calibration products and *Herschel* Interactive Processing Environment (HIPE v12.1.0, Ott 2010) pipelines, with the remainder reduced using SPIRE v10 calibration products +pipelines. We note that measured line fluxes for the two sets of the ∼30% single-pointing data show little difference ($\sigma \sim 8\%$). For single-pointing data, we use central bolometers to extract CO lines. For mapping data, which are usually for spatially-extended galaxies, we select individual bolometers that are >half-beam-separated (Nyquist sampling) to extract CO lines.

Note that FTS covers a wide range of frequencies and its beam size varies accordingly[8]: ∼43″ at CO(4–3) to ∼17″ at CO (13–12), and is not a simple function of frequency. The beam size variation is well-calibrated for each central bolometer, but unavailable for off-axis bolometers. Thus we assign an additional 15% uncertainty for off-axis bolometers.

To derive CO line flux, we use two different line profile fitting functions in HIPE: a Sinc and a Sinc-convolved-Gaussian (SCG). A SCG, where a Gaussian line profile is convolved with the Sinc instrument response, is appropriate for observations of sources with broad/resolved lines (e.g., Zhao et al. 2013): in such cases a Sinc fit would underestimate the line flux by ∼40%. In the more common case where the CO line is not obviously resolved, the SCG-derived fluxes are systematically larger by <20%. Given that a large fraction of single-pointing data have broad/resolved lines while mapping data do not, here we use SCG and Sinc for single-pointing and mapping data, respectively, although we note that using only SCG or Sinc for all data has no significant change to our correlation results. The CO flux uncertainties are derived from the rms in the baseline-subtracted spectra in the vicinity of each CO line rather than from formal line fitting uncertainties. Then the fluxes are converted to $L'_{\rm CO}$ according to Solomon et al. (1992).

2.2. Beam-matched FIR

As a starting point we took the entire-galaxy FIR luminosity ($L_{{\rm FIR},e}$) from Sanders et al. (2003). Given the mismatch between the dramatically varying FTS CO beam sizes and the physical extent of nearby galaxies (e.g., Galametz et al. 2013) and some merging/interacting (U)LIRGs (e.g., Gao & Solomon 1999), we used a beam-scaling method based on the PACS imaging photometry[9] to scale entire-galaxy $L_{{\rm FIR},e}$ down to the local region that matches the CO beam size area ($L_{{\rm FIR},b}$, for each CO line of each bolometer). PACS bands span the peak of the spectral energy distribution (SED) of typical FIR-luminous local galaxies, and thus provide a good proxy for FIR and are insensitive to dust temperatures ($T_{\rm dust}$).[10] By performing photometry with an aperture of CO beam size ($F_{{\rm PACS},b}$) and an aperture of entire-galaxy, ($F_{{\rm PACS},e}$), respectively, we can determine the FIR luminosity that is appropriate to each CO beam size: $L_{{\rm FIR},b} = F_{{\rm PACS},b}/F_{{\rm PACS},e} \times L_{{\rm FIR},e}$.

In this way we calculate a value of $L_{{\rm FIR},b}$ for each CO line. This is essential for local galaxies that are partially resolved for FTS CO beam sizes (e.g., Bayet et al. 2009; Yang et al. 2013; G14; Zhang et al. 2014).

3. RESULTS AND DISCUSSION

3.1. Correlations between $L'_{\rm CO}$ and Beam-matched $L_{\rm FIR}$

Figure 1 shows the 9 CO–FIR correlations of local galaxies and spatially resolved regions of nearby galaxies. FTS can observe CO(4–3) to CO(13–12), except for galaxies at $z > 0.032$ (mostly (U)LIRGs), whose CO(4–3) shift out of the FTS SLW waveband. Moreover, detections of CO(13–12) are sparse, and thus are not analyzed here.

To derive the slope and intercept, we fit all data points (excluding upper limits) with two linear fitting codes: an IDL

[8] Figure 5.18 of http://herschel.esac.esa.int/Docs/SPIRE/spire_handbook.pdf

[9] All PACS data are updated to calibration 48 and post-processed with *Scanamorphos v19.0* (Roussel 2013).

[10] PACS bands: 70, 100, and 160 μm. $\lambda_{\rm peak} \approx 290\ \mu{\rm m}/T_{\rm dust}$, where $T_{\rm dust} \sim$ 20–30 K for typical local SFGs.

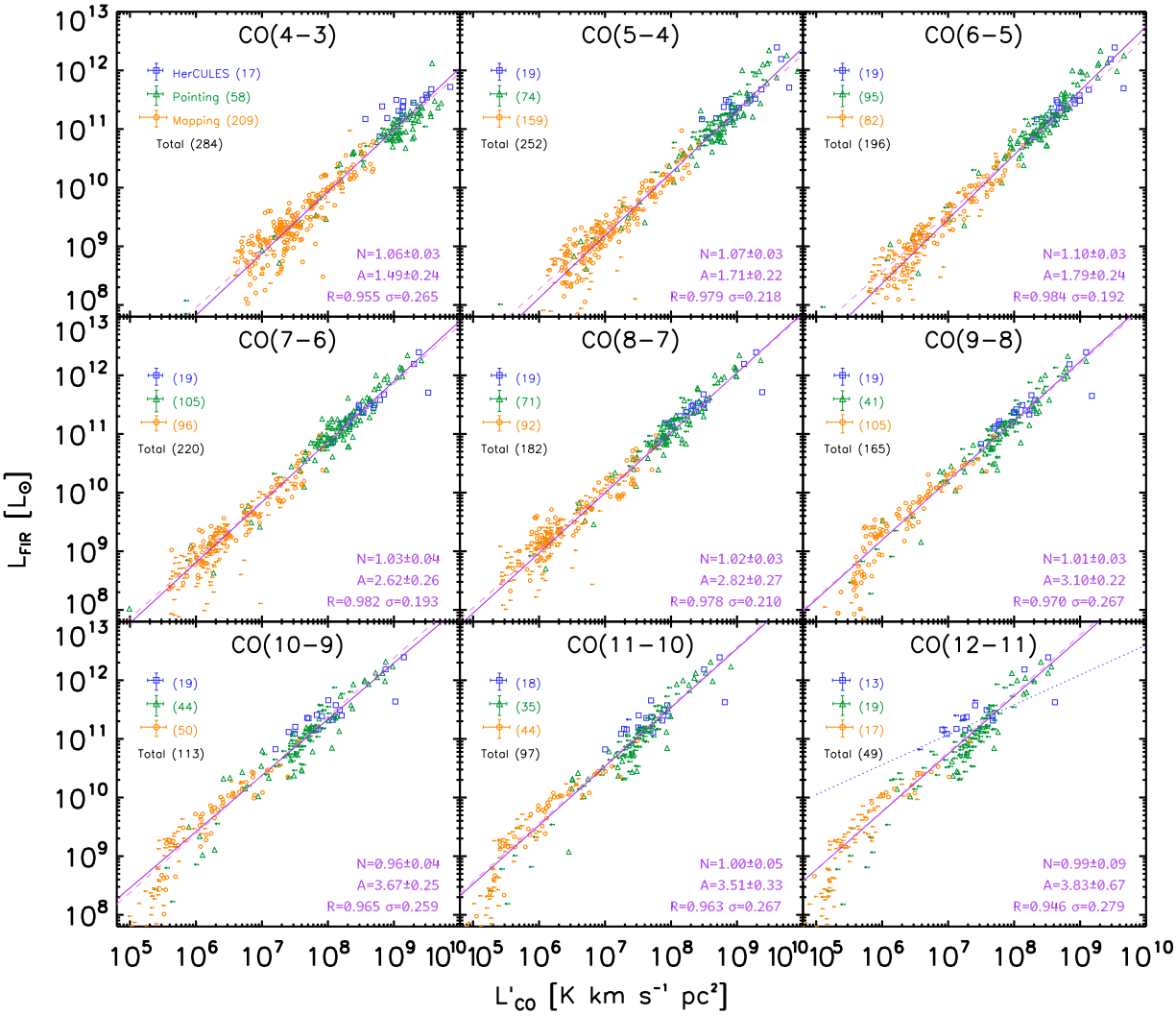

Figure 1. Nine correlations between $L'_{\rm CO}$ and $L_{{\rm FIR},b}$ among local galaxies (blue squares and green triangles) and spatially resolved regions of nearby galaxies (orange circles). The blue squares are from the HerCULES sample, and are the brightest (U)LIRGs. The green triangles are the other single-pointing data, which are less bright, consisting of (U)LIRGs, nearby Seyfert nuclei, and spiral nuclei. The orange circles are the mapping data, of which many are nearby galaxy nuclear regions, but still have some off-nuclear regions at the highest transitions. The numbers of detections for each (sub)sample are shown at the top left, next to the symbol legends. The error bar of each symbol legend is the mean uncertainties of the (sub)sample. The arrows are 3σ upper limits. The best-fitting parameters slope N, intercept A, Pearson correlation coefficient R, and scatter σ (dex) are shown at the bottom right. The solid lines are the best-fit lines with free slopes, while the dashed lines are the best-fit lines with slopes fixed to one, which represent the average $L_{\rm FIR}/L'_{\rm CO}$ for each transition. In the last panel CO(12–11) we show the best-fit line of G14 as a blue dotted line for comparison.

least-squares fitting code based on MPFIT (Markwardt 2009), and an IDL Bayesian regression code LINMIX_ERR (Kelly 2007). The two methods give consistent results, thus we only show the latter results in Figure 1.

CO(4–3) has the largest number of detections, but the least dispersions are seen in the CO(6–5) and CO(7–6) panels (both with $\sigma = 0.19$ dex). This confirms the conclusion of Lu et al. (2014) that CO $J_u \sim$ 6–7 transitions are the best SFR tracers for (U)LIRGs.

For the entire sample, we find no evidence of a significant decrease in slopes with increasing J_u: $N \sim 1.0$–1.1 at $J_u \sim$ 4–6, and 0.96–1.0 at $J_u \sim$ 10–12. Besides, the fittings are consistent with the average distribution of upper limits for non-detections in each transition.

Bayet et al. (2009) analyzed the IR beam corrections based on 850 μm images and found correction factors similar to ours for galaxies we had in common. They found that IR beam corrections have only minor effects on the slopes (<5%) and thus did not apply them, while in contrast we found that slopes without IR beam corrections are smaller by 10%–15%. This partially explains the discrepancy between our results and their decreasing slopes, i.e., $N \sim 1$ at $J_u \sim 3$, then $N \sim 0.8$ at $J_u \sim 7$, and finally $N = 0.53 \pm 0.07$ at $J_u = 12$.

In addition, small number statistics is another key factor behind the discrepancies between different studies. G14 presented the high-J CO–FIR correlation with HerCULES FTS data (Van der Werf et al. 2010) and data from the literature of high-z submillimeter galaxies (SMGs). Their HerCULES sample contains 23 (U)LIRGs (excluding extended/merging galaxies). They evaluate IR beam correction with 870 or 350 μm maps, but the correction factors are small for their local sample (mostly (U)LIRGs). They found correlation slopes $N \sim 1.0$ for $1 \leqslant J_u \leqslant 5$, which then decrease to $N = 0.87 \pm 0.05$ at $J_u = 7$ and then rapidly become $N = 0.51 \pm 0.11$ at $J_u = 12$.

Table 1
Best-fit Parameters of Beam-matched CO–FIR Correlations

(Sub)sample	CO(4–3)	CO(5–4)	CO(6–5)	CO(7–6)	CO(8–7)	CO(9–8)	CO(10–9)	CO(11–10)	CO(12–11)
Entire	$N = 1.06 \pm 0.03$	1.07 ± 0.03	1.10 ± 0.03	1.03 ± 0.04	1.02 ± 0.03	1.01 ± 0.03	0.96 ± 0.04	1.00 ± 0.05	0.99 ± 0.09
	$A = 1.49 \pm 0.24$	1.71 ± 0.22	1.79 ± 0.24	2.62 ± 0.26	2.82 ± 0.27	3.10 ± 0.22	3.67 ± 0.25	3.51 ± 0.33	3.83 ± 0.67
	$\bar{A} = 1.96 \pm 0.07$	2.27 ± 0.07	2.56 ± 0.08	2.86 ± 0.07	3.04 ± 0.08	3.20 ± 0.09	3.38 ± 0.10	3.56 ± 0.11	3.77 ± 0.15
HerCULES	$N = 0.75 \pm 0.62$	1.08 ± 0.43	0.98 ± 0.29	0.84 ± 0.35	0.81 ± 0.24	0.81 ± 0.26	0.73 ± 0.25	0.76 ± 0.26	0.65 ± 0.31
	$A = 4.46 \pm 0.57$	1.67 ± 3.89	2.78 ± 2.61	4.18 ± 3.06	4.68 ± 2.04	4.80 ± 0.21	5.56 ± 0.02	5.49 ± 0.02	6.58 ± 0.00
	$\bar{A} = 2.20 \pm 0.23$	2.40 ± 0.21	2.61 ± 0.21	2.85 ± 0.21	3.08 ± 0.21	3.28 ± 0.22	3.42 ± 0.22	3.65 ± 0.23	3.90 ± 0.28
Pointing	$N = 1.00 \pm 0.10$	1.10 ± 0.09	1.06 ± 0.09	1.05 ± 0.08	1.09 ± 0.11	1.02 ± 0.11	0.93 ± 0.09	1.05 ± 0.12	1.12 ± 0.18
	$A = 1.96 \pm 0.88$	1.43 ± 0.79	2.09 ± 0.79	2.51 ± 0.65	2.34 ± 0.92	3.02 ± 0.84	3.88 ± 0.70	3.12 ± 0.91	2.73 ± 1.36
	$\bar{A} = 1.93 \pm 0.13$	2.30 ± 0.12	2.62 ± 0.11	2.89 ± 0.11	3.02 ± 0.13	3.18 ± 0.16	3.34 ± 0.16	3.51 ± 0.18	3.65 ± 0.24
Mapping	$N = 1.17 \pm 0.10$	1.13 ± 0.09	1.11 ± 0.10	0.96 ± 0.08	0.94 ± 0.08	1.17 ± 0.12	1.12 ± 0.18	1.03 ± 0.17	0.66 ± 0.42
	$A = 0.64 \pm 0.71$	1.29 ± 0.67	1.78 ± 0.74	3.08 ± 0.56	3.44 ± 0.56	2.14 ± 0.77	2.68 ± 1.14	3.40 ± 1.04	5.99 ± 0.00
	$\bar{A} = 1.93 \pm 0.08$	2.22 ± 0.10	2.47 ± 0.13	2.82 ± 0.12	3.04 ± 0.12	3.19 ± 0.12	3.40 ± 0.17	3.58 ± 0.18	3.81 ± 0.29

Note. The best-fit CO—FIR correlations for the 9 transitions. We fit the entire sample and three subsamples separately: G14 HerCULES data, single-pointing data, and mapping data. Both x and y errors are considered. Upper limits are not considered in the fit. N is the best-fit slope and A is the best-fit intercept from free-slope fitting. $\bar{A}$ is the mean FIR/CO ratio ($\bar{A} = \log(L_{\rm FIR}/L'_{\rm CO})$).

For comparison, we divide our entire sample into three subsamples: a HerCULES subsample corresponding to the G14 local sample (mostly (U)LIRGs, excluding extended/merging ones), all other single-pointing data (mixed SFGs+(U)LIRGs), and all mapping data (nearby resolved SFGs, dominating the faint-end). Table 1 lists the best-fit slope N, the intercept A, and the mean FIR/CO ($\bar{A} = \log(L_{\rm FIR}/L'_{\rm CO})$) for the entire sample and three subsamples. For the HerCULES subsample, similar to G14 and Bayet et al. (2009), we find decreasing slopes, e.g., $N = 0.65 \pm 0.31$ at CO(12–11). We overlay the significantly sub-linear CO(12–11)–FIR correlation of G14 ($N = 0.51 \pm 0.11$) in the CO(12–11) panel of Figure 1 for reference.

Thus, with the largest high-J CO data set available to date, we conclude that within the luminosity range shown in Figure 1, $L'_{\rm CO}$ $7 \leqslant J_u \leqslant 9$ closely and linearly follow $L_{\rm FIR}$ and by extension the SFRs, while all other $4 \leqslant J_u \leqslant 12$ CO–FIR correlations are tight and not far from linear. These results are not in conflict with previous studies.

3.2. Average CO/FIR Spectral Line Energy Distribution (SLED)

In Figure 2, we show a global FIR-normalized CO SLED, constructed from the products of the inversion of the best-fit FIR/CO normalization parameter for each transition ($\bar{A}$, which is equal to $L_{\rm FIR}/L'_{\rm CO}$, given in Table 1) $\times J_u^2$ (where J_u^2 is included to make the unit same as integrated line flux Jy km s^{-1}). Error bars are the dispersions of CO–FIR correlations (the σ shown in Figure 1).

This CO SLED represents the average CO excitation conditions in local galaxies, and reveals at least two components: a low-excitation component peaking around $J_u \sim$ 3–4, and a higher-excitation component peaking around $J_u \sim 8$.

We used RADEX (Van der Tak et al. 2007) to construct two-component LVG models and performed least-χ^2 fitting to search for the best fits of gas kinetic temperature $T_{\rm kin}$ and density $n_{\rm H_2}$, deriving $T_{\rm kin} \sim 90^{+100}_{-40}$ K, $\log n_{\rm H_2} \sim 3.0^{+0.3}_{-0.3}$ cm^{-3} for the lower-excitation component, and $T_{\rm kin} \gtrsim 200$ K, $\log n_{\rm H_2} \sim 4.1^{+0.2}_{-0.2}$ cm^{-3} for the higher-excitation component.

In Figure 2, we also overlay the FIR-normalized CO SLEDs of a selection of galaxies that have at least six CO detections

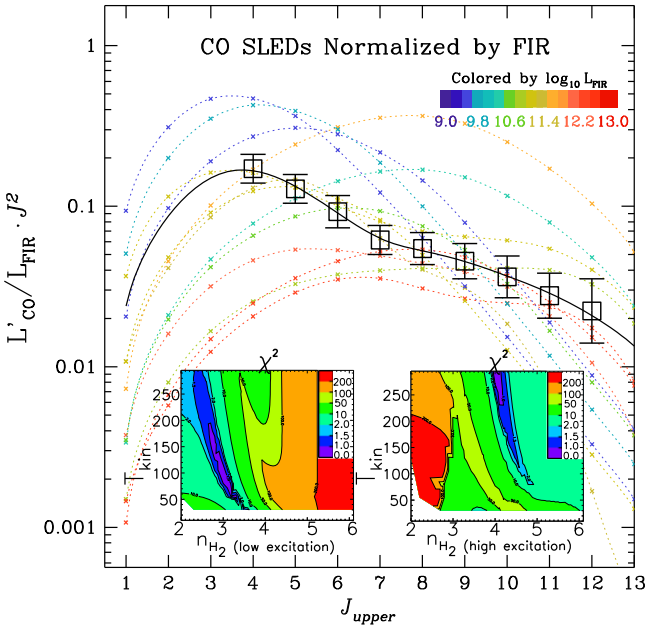

Figure 2. Average CO/FIR SLED (i.e., CO SLED normalized by FIR) for the entire sample, overlaid with several FIR-normalized CO SLEDs of individual galaxies spanning a wide range of $L_{\rm FIR}$. The black open squares are the values of the average CO/FIR (i.e., $L'_{\rm CO}/L_{\rm FIR} \times J_u^2$). The black solid curve is the best-fit two-component LVG model. The other dashed curves are the best-fit one- or two-component LVG models for individual galaxies. The colors indicate their lg($L_{\rm FIR}$). The two embedded panels are the least-χ^2 fitting results of low-excitation gas (left) and high-excitation gas (right), respectively.

and span a wide $L_{\rm FIR}$ range. (U)LIRGs/starbursts have stronger high-J CO excitations and their normalized SLEDs are flatter at $J_u \gtrsim 6$, whereas normal SFGs with weaker excitations show a bump at $J_u \sim 4$ in their normalized SLEDs. Surprisingly, the largest difference between normalized SLEDs of (U)LIRGs and SFGs is seen not at a high-J (i.e., $J_u \sim 10$) but at a low-J (i.e., $J_u \sim 4$), where the CO/FIR ratios vary within $\sim$1.5 dex. Since the low-excitation component dominates the low-J part of SLED, the large variation at a low-J indicates that low-excitation gas is less correlated with FIR, while the high-excitation component is intrinsically better correlated with FIR (see also Lu et al. 2014).

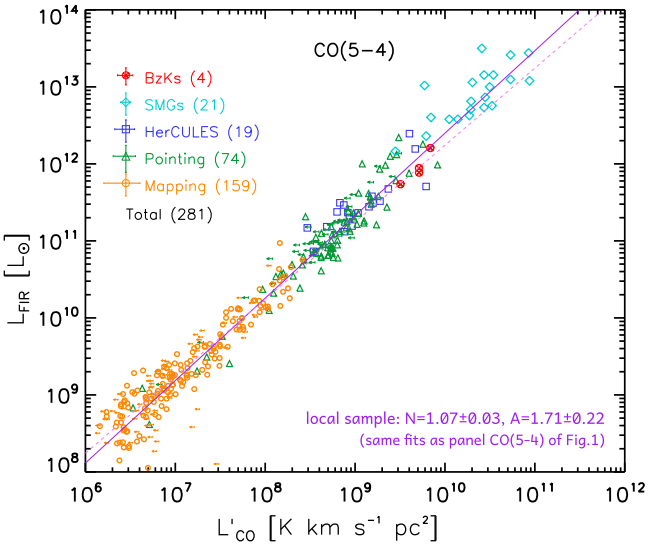

Figure 3. CO(5–4)–FIR correlation including high-z galaxies. The cyan diamonds are high-z galaxies from CW13. The crossed red circles are $z \sim 1.5$ BzKs from Daddi et al. (2015). The other data points and the best fit of the local sample are the same as the CO(5–4) panel of Figure 1.

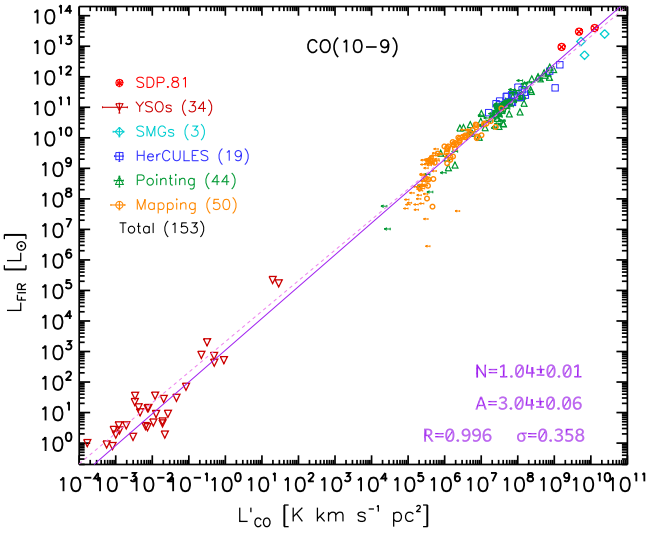

Figure 4. CO(10–9)–FIR correlation, including galactic YSOs/protostars (San José-García et al. 2013, red triangles), high-z SMGs/QSOs (CW13, cyan diamonds), and strongly lensed SMG SDP.81 (global and two components; ALMA Partnership et al. 2015, red crossed circles). The three data points of SDP.81 are: the west component, the east component, and global, from left to right, respectively. The solid line is a free-slope fit for all sources. The dashed line is a fixed-slope $N = 1$ fit, indicating a mean $\log(L_{\rm FIR}/L'_{\rm CO(10-9)}) = 3.30 \pm 0.09$.

3.3. The CO(5–4)—FIR Correlation and Extension to High-z

To extend the high-J CO–FIR correlation toward higher-z, we use the extensive compilation of high-z CO data in CW13 that contains 60 CO $J_u \geqslant 4$ detections with literature $L_{\rm IR}$.[11] They are the most extreme starbursts across all cosmic time, likely experiencing a short-term burst phase of SF resembling local ULIRGs, rather than the long-lasting mode in normal SFGs or the so-called "main-sequence" (MS) galaxies at high-z (e.g., CW13).

CO $J_u \geqslant 4$ observations toward high-z MS galaxies are still very rare: Daddi et al. (2015) presented the first CO(5–4) detections in a sample of 4 $z \sim 1.5$ BzK-color-selected MS galaxies (BzKs). Thus combining all high-z $J_u \geqslant 4$ data, CO (5–4) has the second-most detections but covers the most diverse galaxy types.

In Figure 3, we show the CO(5–4)—FIR correlation, including high-z galaxies as an example to illustrate the correlation between dense gas and SFR, as CO(5–4) traces a hundred times denser molecular gas than CO(1–0). We show the linear fits from Figure 1 only, as the inclusion of high-z SMGs and BzKs does not significantly change the results of the fit. The mean $\log(L_{\rm FIR}/L'_{\rm CO(5-4)}) = 2.27 \pm 0.07\ L_\odot\ ({\rm K\ km\ s^{-1}\ pc^2})^{-1}$ is consistent with Daddi et al. (2015) considering a conversion factor of 1/1.3 from TIR to FIR. BzK galaxies fall on the local linear best-fit correlation (dashed line), whereas high-z SMGs are offset above by ∼0.28 dex. Interestingly, using HCN(1–0) as a dense gas tracer, Gao et al. (2007) found higher FIR/HCN ratios in high-z galaxies (mostly QSOs/AGNs with only 5 HCN detections) than those of local ULIRGs/SFGs.

[11] The $L_{\rm FIR}$ for nine galaxies are derived from IR SEDs, a further 14 from FIR-radio correlation (Bothwellet al. 2013; CW13), and the remaining 37 scaled from single-band 850 or 1200 μm (CW13; Greve et al. 2014). Where required we converted $L_{\rm TIR}$ to $L_{\rm FIR}$ by a factor of 1/1.3.

[12] For example, 850 μm-derived $L_{\rm FIR}$ (using CW13 conversion factor) are ∼77%–200% of radio-derived $L_{\rm FIR}$ in Bothwell et al. (2013). Lensing corrections also introduce uncertainties.

Given the large uncertainties in $L_{\rm FIR}$ for a large fraction of SMGs[12] compared to BzKs (from SED fitting), the amount of excess in FIR/CO(5–4) (i.e., dense gas SF efficiency) in SMGs should still be treated with caution. And this excess is not significant enough to break down a linear form of dense gas versus SF relation, as these starbursts are the most extreme systems at all redshifts and as such do not represent the dominant mode of SF observed in MS galaxies (e.g., BzKs). Thus, better FIR measurements, e.g., via SEDs, and additional high-J CO observations in normal MS galaxies are needed before making solid conclusions at high-z.

3.4. The CO(10–9)—FIR Correlation Extending to Galactic Young Stellar Objects (YSOs)

In Figure 4 we show the correlation between an even denser/warmer gas tracer CO(10–9) and $L_{\rm FIR}$, which has the largest number of observations of sources, spanning high-z galaxies (from CW13 and ALMA Partnership et al. 2015) to galactic YSOs/protostars (from San José-García et al. 2013).

ALMA Partnership et al. (2015) presented spatially resolved ALMA CO(10–9) in a strongly lensed SMG SDP.81 at $z = 3.042$, with demagnified $L_{\rm TIR} = 5.1 \times 10^{12}\ L_\odot$, comparable to the BzKs. We show the global SDP.81 as well as its east and west components in Figure 4.

The best fit for all sources is $N = 1.04 \pm 0.01$ and $A = 3.04 \pm 0.06$ (see also San José-García et al. 2013, who obtained the same $N = 1.04$ with only six galaxies); considering YSOs/protostars alone we get $N = 1.26 \pm 0.09$, which is likely biased by the limited number of bright sources ($L_{\rm bol} \approx 10^5\ L_\odot$). A fixed-slope $N = 1$ fit indicates that a mean $\log(L_{\rm FIR}/L'_{\rm CO(10-9)}) = 3.30 \pm 0.09\ L_\odot\ ({\rm K\ km\ s^{-1}\ pc^2})^{-1}$ is valid for all sources within $\sigma \sim 0.36$ dex.

3.5. Conclusions

We use *Herschel* SPIRE FTS observations of 167 local galaxies, including mapping data, to determine $L'_{\rm CO}$ $J = 4$–3 to 12–11, and derive corresponding beam-matched $L_{{\rm FIR},b}$ for each CO line using PACS photometry. We find that these CO–FIR correlations are all linear, and that the non-linear result reported in G14 can be attributed to the comparatively small number of galaxies in their sample. The overall linearity suggests that a universal CO/FIR SLED exists among these galaxies, which further reveals two excitation states of gas. The high-excitation CO SLED peaks at $J \sim 7$, where the transitions are the best tracers of SFR (e.g., Lu et al. 2014).

At high-z, however, SMGs/QSOs have elevated FIR/CO (5–4) ratios relative to those seen in local galaxies and contemporary BzKs: this is because they are the most extreme types of galaxies and hence are not representative of the typical SFG population.

A tight, linear correlation between CO(10–9)–FIR is shown to hold for the majority of local galaxies, resolved sub-kpc regions, Galactic YSOs, and also high-z galaxies. These results strongly support a fundamental linear relationship between dense gas and the SFR, and also provide the local benchmark for probing the gas and SF in more types of galaxies (e.g., MS galaxies) at high-z.

This work is supported by NSFC #11173059, #11390373, #11420101002, and CAS #XDB09000000. D.L. gratefully thanks T. Greve, Z. Zhang, P. Papadopoulos, S. Madden, and R. Wu for constructive discussions, and K. Okumura and B. Altieri for helpful instructions on PACS.

REFERENCES

ALMA Partnership, Vlahakis, C., Hunter, T. R., et al. 2015, ApJL, 808, L4
Aniano, G., Draine, B. T., Gordon, K. D., & Sandstrom, K. 2011, PASP, 123, 1218
Bayet, E., Gerin, M., Phillips, T. G., & Contursi, A. 2009, MNRAS, 399, 264
Bigiel, F., Leroy, A., Walter, F., et al. 2008, AJ, 136, 2846
Bothwell, M., Smail, I., Chapman, S., et al. 2013, MNRAS, 429, 3047
Carilli, C. L., & Walter, F. 2013, ARA&A, 51, 105
Daddi, E., Dannerbauer, H., Liu, D., et al. 2015, A&A, 577, A46
Daddi, E., Elbaz, D., Walter, F., et al. 2010, ApJL, 714, L118
Galametz, M., Kennicutt, R. C., Calzetti, D., et al. 2013, MNRAS, 431, 1956
Gao, Y., Carilli, C. L., Solomon, P. M., & Vanden Bout, P. A. 2007, ApJL, 660, L93
Gao, Y., & Solomon, P. M. 1999, ApJL, 512, L99
Gao, Y., & Solomon, P. M. 2004, ApJ, 606, 271
Greve, T. R., Bertoldi, F., Smail, I., et al. 2005, MNRAS, 359, 1165
Greve, T. R., Leonidaki, I., Xilouris, E. M., et al. 2014, ApJ, 794, 142
Griffin, M. J., Abergel, A., Abreu, A., et al. 2010, A&A, 518, L3
Iono, D., Wilson, C. D., Yun, M. S., et al. 2009, ApJ, 695, 1537
Juneau, S., Narayanan, D. T., Moustakas, J., et al. 2009, ApJ, 707, 1217
Kennicutt, R. C. 1998, ApJ, 498, 541
Kennicutt, R. C., Jr., & Evans, N. J. 2012, ARA&A, 50, 531
Krumholz, M. R., & McKee, C. F. 2005, ApJ, 630, 250
Krumholz, M. R., & Thompson, T. A. 2007, ApJ, 669, 289
Kelly, B. C. 2007, ApJ, 665, 1489
Liu, L., & Gao, Y. 2012, ScChG, 55, 347
Liu, L., Gao, Y., & Greve, T. R. 2015, ApJ, 805, 31
Lu, N., Zhao, Y., Xu, C. K., et al. 2014, ApJL, 787, L23
Mac Low, M. M., & Klessen, R. S. 2004, RvMP, 76, 125
Mao, R., Schulz, A., Henkel, C., et al. 2010, ApJ, 724, 1336
Markwardt, C. B. 2009, in ASP Conf. Ser. 411, Astronomical Data Analysis Software and Systems XVIII, ed. D. A. Bohlender, D. Durand, & P. Dowler (San Francisco, CA: ASP), 251
Narayanan, D., Cox, T. J., Shirley, Y., et al. 2008, ApJ, 684, 996
Naylor, D. A., Baluteau, J.-P., Barlow, M. J., et al. 2010, Proc. SPIE, 7731, 773116
Ott, S. 2010, in ASP Conf. Ser. 434, Astronomical Data Analysis Software and Systems XIX, ed. Y. Mizumoto, K.-I. Morita, & M. Ohishi (San Francisco, CA: ASP), 139
Papadopoulos, P. P., Van der Werf, P., Xilouris, E. M., et al. 2012, MNRAS, 426, 2601
Pineda, J. L., Langer, W. D., & Goldsmith, P. F. 2014, A&A, 570, 121
Poglitsch, A., Waelkens, C., Geis, N., et al. 2010, A&A, 518, L2
Rosenberg, M., van der Werf, P., Aalto, S., et al. 2015, ApJ, 801, 72
Roussel, H. 2013, PASP, 125, 1126
Sanders, D. B., Mazzarella, J. M., Kim, D. C., Surace, J. A., & Soifer, B. T. 2003, AJ, 126, 1607
San José-García, I., Mottram, J. C., Kristensen, L. E., et al. 2013, A&A, 553, A125
Schruba, A. 2013, IAUS, 292, 311
Solomon, P. M., Downes, D., & Radford, S. J. E. 1992, ApJL, 398, L29
Springel, V., & Hernquist, L. 2003, MNRAS, 339, 289
Van der Werf, P. P., Isaak, K. G., Meijerink, R., et al. 2010, A&A, 518, L42
Van der Tak, F. S., Black, J. H., Schöier, F. L., et al. 2007, A&A, 468, 627
Vogelsberger, M., Genel, S., Springel, V., et al. 2014, MNRAS, 444, 1518
Wu, J., Evans, N., Gao, Y., et al. 2005, ApJ, 635, L173
Wu, J., Evans, N., Shirley, Y. L., & Knez, C. 2010, ApJS, 188, 313
Yang, C., Gao, Y., Omont, A., et al. 2013, ApJ, 771, L24
Zhang, Z., Gao, Y., Henkel, C., et al. 2014, ApJ, 784, L31
Zhao, Y., Lu, N., Xu, C. K., et al. 2013, ApJ, 765, L13